Composites Science and Technology 218 (2022) 109190

Contents lists available at ScienceDirect

Composites Science and Technology

journal homepage: www.elsevier.com/locate/compscitech

Protective performance and dynamic behavior of composite body armor with shear stiffening gel as buffer material under ballistic impact

Fan Tang [a,d,1], Cheng Dong [a,d,1], Zhe Yang [b], Yue Kang [c], Xiancong Huang [c], Maohui Li [c], Yuchao Chen [a,d], Wenjian Cao [a], Chenguang Huang [a], Yacong Guo [a,**], Yanpeng Wei [a,*]

[a] Key Laboratory for Mechanics in Fluid Solid Coupling Systems, Institute of Mechanics, Chinese Academy of Sciences, Beijing, 100190, China
[b] Shandong We Are So Young Protection Technology Co. Ltd., Yantai, 265500, China
[c] The Quartermaster Research Institute of Engineering and Technology, Beijing, 100010, China
[d] School of Engineering Science, University of Chinese Academy of Sciences, Beijing, 100049, China

ARTICLE INFO

Keywords:
Shear stiffening gel
Protective performance
Dynamic behavior
Composite body armor

ABSTRACT

To solve the problem of insufficient protective performance of the existing body armor, an impact-resistant shear stiffening gel (SSG) with excellent flexibility and formability was innovatively used as buffer plate for body armor, and then combined with ultra-high molecular weight polyethylene (UHMWPE) ballistic panel to form a UHMWPE/SSG composite body armor. Based on the ballistic impact experiment and numerical simulation, the effect of buffer plate on the protective performance, and the dynamic behavior and protective mechanism of UHMWPE/SSG were analyzed systematically. The results indicated that the flexible SSG buffer plate could quickly stiffen under ballistic impact, thereby producing the strong "Jamming" effect to resist impact deformation and absorb impact energy. Moreover, the "Jamming" effect enhanced with the increase of impact load, and showed a distribution mode that weakened from the ballistic impact area to the periphery. Compared with traditional buffer materials, more impact energy was dispersed and absorbed by SSG, but less impact energy was transmitted to the human body. Therefore, the impact strength of UHMWPE/SSG on the human body and backface signature of human body were also significantly reduced (up to 50%), which showed that the composite body armor with SSG buffer material exhibited superior protective performance.

1. Introduction

Body armor is a kind of personal protective equipment that effectively protects the human body from gunshot hazards by absorbing the impact energy of bullets [1,2]. According to the protection objects of body armor, its performance is described as ballistic performance and protective performance. As the primary objective, ballistic performance represents the penetration ability of body armor against bullet. The protective performance is the ultimate objective, which indicates the protective ability of body armor to the human body. A lot of evidence shows that the existing body armor has excellent ballistic performance and can avoid penetrating injury [3,4]. However, the impact energy of bullet is difficult to be completely absorbed by the body armor, so that part of the impact energy is transmitted to the human body, resulting in blunt injury to the human body, that is, behind armor blunt armor (BABT) [5,6].

The protective performance of body armor is always the key issue of personal protective equipment, but it has not been paid enough attention. With the rapid development of personal protective equipment, the protection goal of body armor has upgraded from reducing BABT to maintaining combat effectiveness after BABT. To improve the protective performance of body armor, the most feasible method is to add a buffer material on the back of the ballistic panel to further weaken the impact strength of body armor on the human body. Therefore, the energy-

; SSG, Shear stiffening gel; UHMWPE, Ultra-high molecular weight polyethylene; BABT, Behind armor blunt armor; EVA, Ethylene-vinyl acetate copolymer; PU, Polyurethane; STM, Shear thickening material; STF, Shear thickening fluid; CBA, Composite body armor; EHB, Equivalent human body; BFS, Backface signature; FEM, Finite element model; MIF, Maximum impact force.

* Corresponding author.
** Corresponding author.
E-mail addresses: guoyacong@imech.ac.cn (Y. Guo), weiyanpeng@imech.ac.cn (Y. Wei).

[1] Contributed equally in this work.

https://doi.org/10.1016/j.compscitech.2021.109190
Received 2 October 2021; Received in revised form 9 November 2021; Accepted 29 November 2021
Available online 30 November 2021

absorbing materials, such as ethylene-vinyl acetate copolymer (EVA) and polyurethane (PU), were widely used as buffer plate to further reduce BABT. However, practical applications showed that traditional buffer materials were still difficult to effectively reduce BABT [7]. Consequently, it is urgent to develop a buffer material with more excellent impact resistance to form effective protection for the human body.

As a non-Newtonian fluid, the shear thickening materials (STM) with excellent protection, comfort and flexibility are widely used in the field of personal protection, such as liquid body armor [8,9]. STM presents a low-viscosity fluid-like state with excellent flexibility under no impact load, but the viscosity of STM increases sharply and presents a solid-like state to absorb impact energy under impact load [10,11].

STM mainly includes shear thickening fluid (STF) and shear stiffening gel (SSG). As the most common shear thickening materials, STF can greatly increase the friction between fiber yarns, so that it is usually used to impregnate the ballistic fiber to improve its ballistic performance [12–14]. Although many studies have confirmed that STF can significantly enhance the ballistic performance of fibers, but the significant liquidity of STF greatly restricts its application [15,16]. By comparison with STF, SSG not only exhibits excellent flexibility and impact resistance, but also presents gel properties with superior formability under normal conditions [17–19]. Zhao et al. [20] analyzed the impact resistance of SSG-Kevlar composites and revealed its dynamic mechanical properties and energy absorption mechanism. Xu et al. [21] studied the ballistic performance of the Kevlar/SSG composites, and analyzed its energy absorption. Wang et al. [22,23] investigated the dynamic mechanical properties, shear hardening and self-healing mechanism of SSG, and established constitutive parameters based on the Cowper-Symonds model. Liu [17,24] et al. compounded SSG to PU, and found that the impact resistance and energy absorption performance of PU was significantly enhanced. He et al. [25] impregnated Kevlar with STF and then smeared with SSG, and found that SSG further improved the impact resistance of STF/Kevlar material.

The objective of this study was to develop a smart SSG buffer materials for body armor, and then form a UHMWPE/SSG composite body armor (CBA) by combining with multilayer ultra-high molecular weight polyethylene (UHMWPE) to evaluate its application prospects in the field of personal protection. Based on the combined method of ballistic impact experiment and numerical simulation, the dynamic behavior and protective mechanism of UHMWPE/SSG were emphatically analyzed.

2. Materials and methods

2.1. Preparation and mechanical properties of SSG

Fig. 1a shows the preparation process of SSG. First, boric acid (H_3BO_3) and hydroxyl-terminated polydimethylsiloxane (PDMS-OH) were used as raw materials and mixed uniformly in a breaker at a weight ratio of 1:5. Then, the mixture was stirred at a high temperature of 160–180 °C for 2–3 h to synthesize polyborosiloxane with a mass density of 1.08 g/cm^3. Finally, SSG material with low fluidity and excellent formability was obtained after cooling.

The dynamic mechanical analysis was used to characterize the stiffening behavior of SSG (diameter = 1.5 cm, height = 0.7 cm) under dynamic load, as shown in Fig. 1b. Obviously, as the frequency increased, the elastic modulus of SSG increased significantly, but its viscous modulus gradually decreased after reaching a peak, which indicated that SSG undergo a phase transition from viscous state to elastic state. Therefore, SSG could absorb and store more impact energy under high-velocity impact.

2.2. Compound mode of body armor

CBA was comprised of ballistic panel, buffer plate and backplate, as shown in Fig. 2a. Both the ballistic panel and the backplate were made of UHMWPE laminates with a thickness of 0.015 cm. Considering the importance of heart protection, and the lightweight requirements of body armor. The SSG buffer plate with a diameter of 10 cm was made by a Teflon mold and encapsulated in front of the heart for enhanced protection, and the other parts were EVA material. Finally, a UHMWPE/SSG composite body armor (Fig. 2b) with an areal density of 5.38 kg/m^2 was obtained. To verify the protective performance of SSG buffer material, the traditional EVA buffer material was used as a reference, and combined with UHMWPE to form a UHMWPE/EVA composite body armor (Fig. 2c) with an areal density of 4.93 kg/m^2.

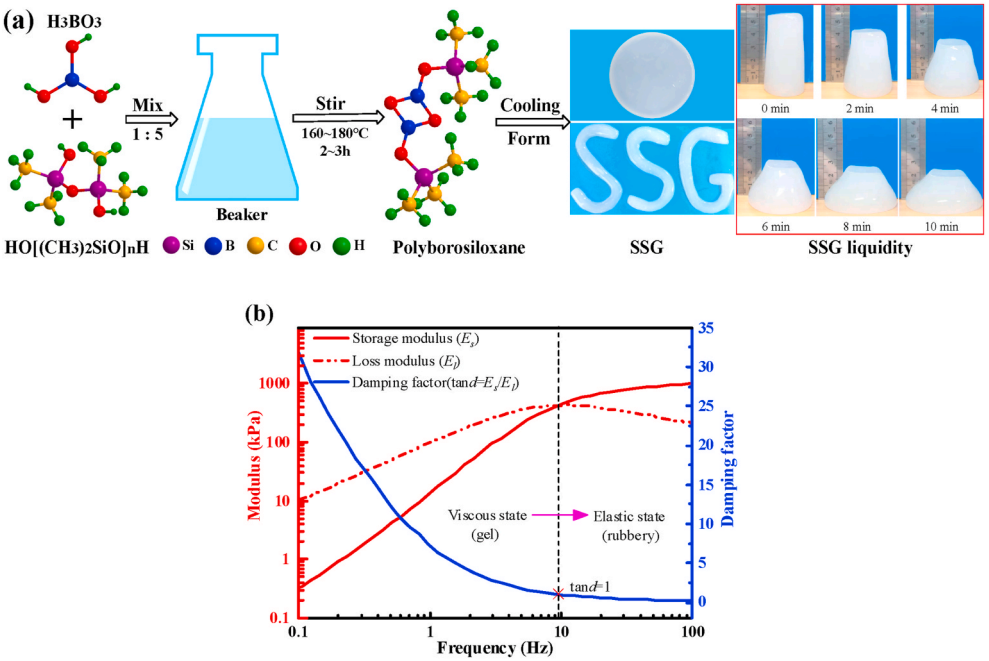

Fig. 1. SSG: (a) preparation process and (b) dynamic mechanical properties.

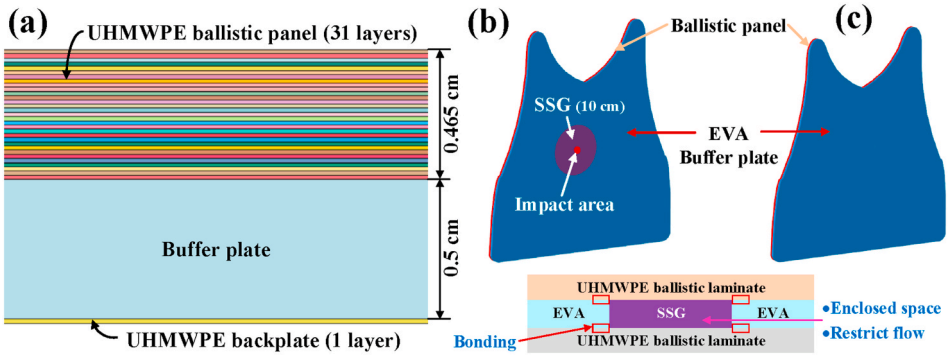

Fig. 2. CBA: (a) compound mode, (b) UHMWPE/SSG and (c) UHMWPE/EVA.

2.3. Ballistic impact experiment platform

The ballistic impact experiment platform is shown in Fig. 3. According to Chinese GA-2 protection standard (equivalent to US NIJ-IIIA) of body armor, a 7.62 mm bullet with a mass of 5.60 g and an initial velocity of 445 ± 10 m/s was used. The ballistic clay was regarded as an equivalent human body (EHB), and the protective performance of CBA was evaluated by the backface signature (BFS: GA-25 mm & NIJ-44 mm) of EHB. The high-speed camera was used to capture the impact process of the bullet on the CBA. Tekscan® distributed pressure sensor was placed between CBA and EHB, and its central element was located exactly at the preset ballistic impact area. After the ballistic impact, the validity of the measurement was judged by checking whether the actual ballistic impact area was consistent with the preset ballistic impact area.

2.4. Protective performance of CBA

Fig. 4 presents the response and distribution of impact pressure obtained by the ballistic impact experiments. The impact pressure response of UHMWPE/EVA and UHMWPE/SSG first increased sharply and then decreased slowly, but the evolution of the impact pressure distribution presented a significantly different pattern.

The impact pressure of UHMWPE/EVA was concentrated at the impact area, showing the "mountain" distribution with high center and low periphery (Figs. 4a–1&**2**). After the ballistic impact of bullet was over, UHMWPE/EVA continued to impact EHB and showed uneven deformation, resulting in insufficient contact with EHB, so the impact pressure presented a discontinuous distribution (Figs. 4a–3&**4**).

The impact pressure of UHMWPE/SSG presented the "mountain" distribution at the beginning of the ballistic impact (Figs. 4b–1). Subsequently, the impact pressure gradually spread from the impact area to the periphery, presenting the "valley" distribution with low center and high periphery (Figs. 4b–2&**3**). This indicated that SSG at the impact area produced impact stiffening phenomenon, which dispersed the impact energy around the impact area, thereby reducing the impact pressure at the impact area. After the ballistic impact, the impact strength was gradually weakened (Fig. 4b–).

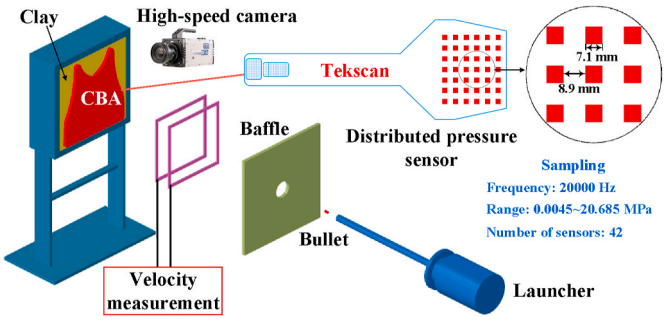

Fig. 3. Ballistic impact experiment platform.

Table 1 compared the protective performance of CBA. The experimental results showed that the ballistic impact exhibited satisfactory repeatability. CBA produced severe bulge deformation, but only 4–5 layers of UHMWPE ballistic laminates were damaged, which proved the excellent ballistic performance of CBA. Compared with UHMWPE/EVA, UHMWPE/SSG was impacted by higher-velocity bullet, but the impact force and impact pressure at the impact area were both reduced by 45% from 0.73 kN to 0.40 kN and from 2861.61 kPa to 1571.08 kPa, and BFS was decreased by 48% from 1.07 cm to 0.56 cm, which indicated that the SSG buffer plate presented significant advantages in improving the protective performance of body armor.

3. Numerical simulation

3.1. Finite element model (FEM)

FEM was established by HyperMesh 2021 software, and LS-DYNA R11 software was used to simulate the impact process. FEM consisted of air, bullet, ballistic panel, buffer plate and EHB, which were modeled as hexahedral elements, as shown in Fig. 5.

The "Arbitrary Lagrangian Eulerian" algorithm was applied for air, the "Lagrange" algorithm was used for other parts, and the fluid-structure interaction was adopted between air and other parts. Considering the symmetry and computational efficiency of FEM, a quarter FEM was established. On the premise that the mesh sensitivity was carefully studied in advance to ensure the numerical convergence, the elements of CBA and EHB at the impact area were encrypted, and the element size of the entire FEM increased from the impact area to the surroundings. The eroding contact was used between bullet and CBA, and the automatic contact was applied to CBA and EHB.

3.2. Material models and properties

The "Null" material model and "Linear Polynomial" equation of state were used for air, its material parameters were derived from Ref. [26]. The bullet was composed of steel jacket and lead core, which were modeled using the "Johnson-Cook" material model and "Gruneisen" equation of state, its material parameters were derived from Ref. [27]. As an orthotropic material, the "Composite Material" constitutive model and "Maximum Principal Strain" damage criterion were applied to UHMWPE, its material parameters were shown in Table 2. The "Power Law Plasticity" material model was used to simulate EHB, its material parameters were given in Table 3.

For EVA material, the "Low Density Foam" material model [30] was selected, with the density of 0.03 g/cm^3, the elastic modulus of 2.4 MPa, and the Poisson ratio of 0.33. The Cowper-Symonds model [23,31], an elastic-plastic isotropic-kinematic hardening material model, was employed to describe the strain rate effects of SSG. The elastic modulus was 60 Pa, the Poisson's ratio was 0.49, and the yield stress (σ_y) was:

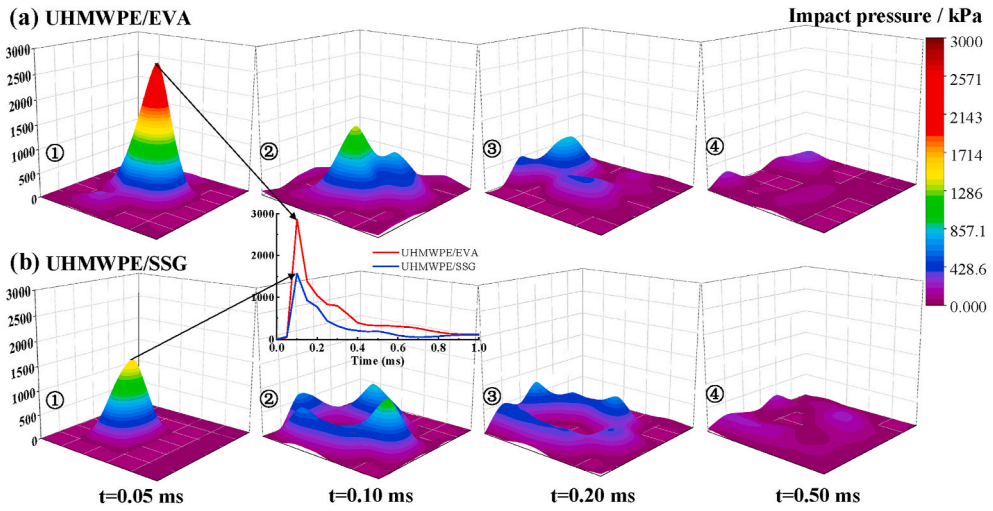

Fig. 4. Impact pressure: (a) UHMWPE/EVA and (b) UHMWPE/SSG.

Table 1
Protective performance of CBA.

CBA	Impact velocity (m/s)	Impact force (kN)	Impact pressure (kPa)	BFS (cm)
UHMWPE/EVA	440.22	0.73	2861.61	1.07
	440.08	0.71	2780.38	1.06
UHMWPE/SSG	453.72	0.40	1571.08	0.56
	455.48	0.41	1615.97	0.58

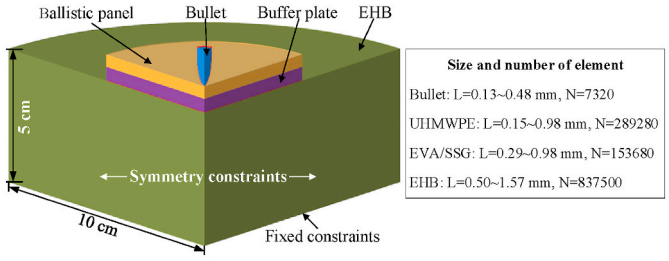

Fig. 5. Ballistic impact finite element model.

Table 2
Material parameters of UHMWPE ballistic laminate [28].

ρ	Ea	Eb	Ec	Gab	Gbc	Gca	νab	νbc
0.97 g/cm3	40.6 GPa		2.6 GPa	1.75 GPa	1.6 GPa		0.008	0.044
νca	K	SC	YC	XT	YT	SN	SYZ	SZX
0.044	2.2 GPa	0.5 GPa	3 GPa	3.6 GPa		0.9 GPa		

Table 3
Material parameters of EHB [29].

ρ	E	σy	ν	K	N
1.539 g/cm3	5.347 MPa	0.01 MPa	0.49	0.3609 MPa	0.1649

$$\sigma_y = \left[1 + \left(\frac{\dot{\varepsilon}}{C}\right)^{\frac{1}{P}}\right]\left[A + B\varepsilon_{eff}{}^{n}\right] = \left[1 + \left(\frac{\dot{\varepsilon}}{0.001012}\right)^{\frac{1}{1.06}}\right]\left[44.64 + 21.795\varepsilon_{eff}{}^{0.622}\right] \quad (1)$$

where C and P are strain rate parameters, A is the initial yield stress, B is the plastic hardening parameter, $\dot{\varepsilon}$ is the effective plastic strain rate and ε_{eff}^{p} is the effective plastic strain.

3.3. Validation of FEM

The impact force of CBA and backface signature of EHB at the impact central area were compared, as shown in Fig. 6. The response of impact force and the damaged layers of UHMWPE ballistic laminate were in good agreement with experiment data. For the UHMWPE/EVA, the relative error of maximum impact force (MIF) and BFS were 5.48% and 4.67%. For the UHMWPE/SSG, the relative error of MIF and BFS were 7.50% and 5.36%. These satisfactory verification results indicated that FEM could effectively simulate the dynamic behavior of CBA under ballistic impact.

4. Results and discussion

Under the ballistic impact velocity of 445 m/s (GA-2 protection), the ballistic impact process of bullet and the dynamic behavior of CBA were analyzed.

4.1. Deformation mode and process

Fig. 7 displays the deformation mode and process of ballistic impact model. Obviously, UHMWPE ballistic laminate subjected to ballistic impact produced tensile and shear failures, and the back of UHMWPE ballistic laminate mainly showed tensile and shear deformation, so that a non-penetrating bullet hole was formed in the UHMWPE ballistic panel. The buffer plate and backplate produced tensile, shear and compressive deformation, and finally a backface signature was formed on the EHB.

According to the deformation characteristics of CBA and EHB, the deformation curves of CBA and EHB showed exactly the same response in the early stage of ballistic impact, which was caused by the direct contact impact of CBA on EHB. When the impact of CBA on EHB was over, CBA reached the maximum bulge deformation and started to rebound, so the deformation curve showed a downward trend. However, due to the influence of the inertial motion effect, the inward concave deformation of EHB continued to increase, and remained stable after

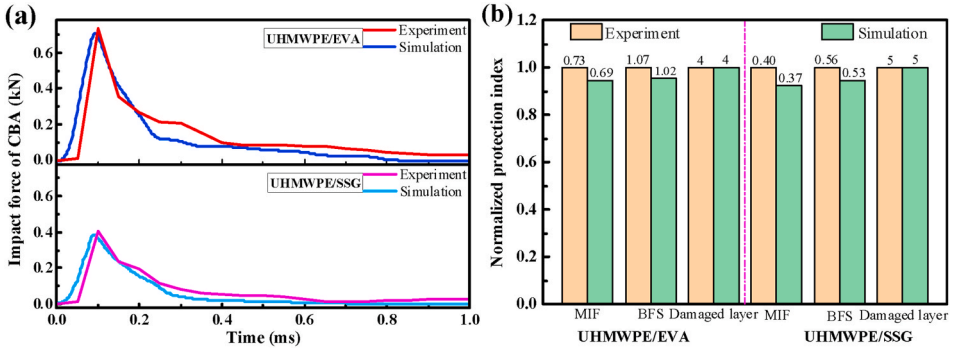

Fig. 6. Validation of FEM: (a) impact response and (b) normalized comparison.

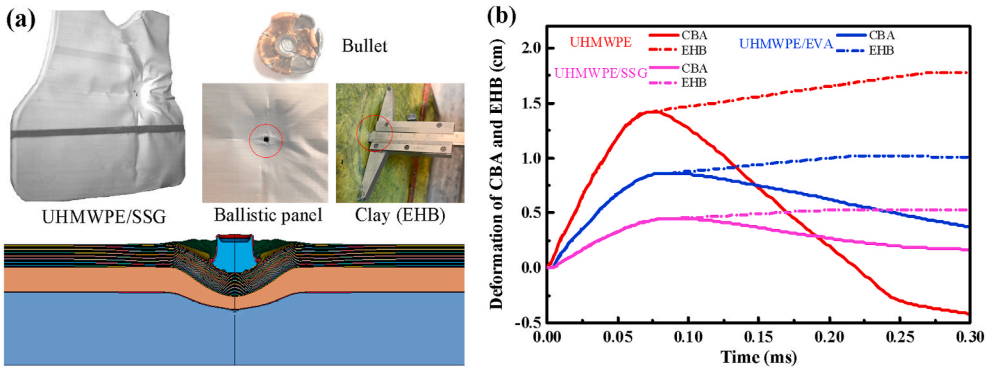

Fig. 7. Ballistic impact model: (a) deformation mode and (b) deformation process.

reaching the maximum backface signature. Ultimately, the backface signature of EHB was slightly larger than the maximum bulge deformation of CBA. The difference between the bulge deformation of CBA and the backface signature of EHB mainly depended on the impact strength of CBA on EHB, and increased as the impact strength increased.

It was worth noting that the maximum bulge deformation of UHMPWE was significantly higher than UHMWPE/EVA and UHMWPE/SSG, which indicated that the individual ballistic panel was not enough to effectively protect the human body. Therefore, it was necessary to use the buffer plate for the body armor to achieve further enhanced protection.

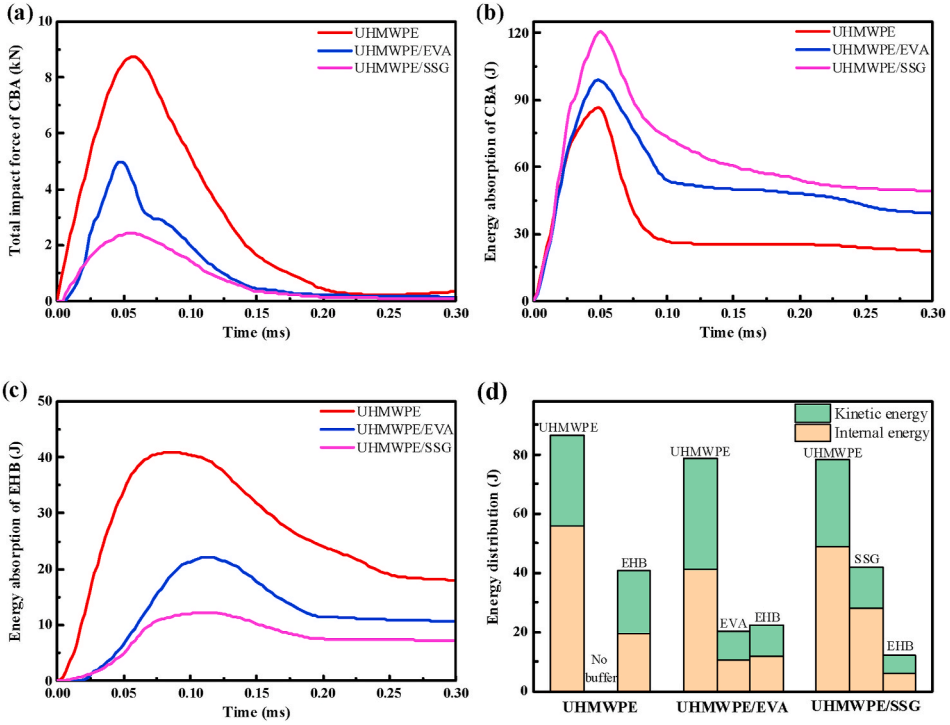

Fig. 8. Ballistic impact model: (a) total impact force and (b) energy absorption of CBA, (c) energy absorption of EHB and (d) energy distribution of each component.

4.2. Impact strength and energy absorption

Fig. 8 presents the impact strength and energy absorption of CBA. The ballistic impact energy was mainly dissipated as follows. (1) the transfer of impact kinetic energy of bullet to internal energy; (2) the deformation and failure of UHMWPE ballistic panel; (3) the deformation of buffer plate and EHB; (4) the friction between bullet and ballistic panel.

The impact force of CBA showed a similar response process, but the maximum impact force of UHMWPE (8.74 kN) was higher than that of UHMWPE/EVA (5.00 kN) and UHMWPE/SSG (2.42 kN), which were 1.75 times that of UHMWPE/EVA and 3.61 times that of UHMWPE/SSG. For the UHMWPE without buffer plate, although CBA absorbed most of the impact energy (86.46 J), it also transferred a relatively high impact energy to EHB (40.92 J). For the UHMWPE/EVA and UHMWPE/SSG with buffer plate, CBA not only absorbed more impact energy (98.77 J and 120.39 J), but also transmitted less impact energy to EHB (22.18 J and 12.14 J).

From the perspective of energy distribution, the energy absorption of CBA was dominated by internal energy. Among them, the ballistic panel absorbed the most impact energy, followed by the buffer plate, while EHB absorbed the lowest impact energy. By comparing the energy absorption of EVA and SSG, it could be obtained that the energy absorption performance of SSG (42.07 J) was not only better than that of EVA (20.13 J), but also had a higher proportion (66.29%) of internal energy than EVA (51.37%), which indirectly indicated that SSG had better damping performance.

4.3. Propagation and attenuation of stress wave

During the ballistic impact, the stress waves generated by the bullet impact simultaneously propagated in the CBA as the transverse wave and longitudinal wave.

According to the stress wave theory [32], it was obtained that the velocity of stress wave and the elastic impedance of material were significantly affected by the elastic modulus of material, and increased with the increase of the elastic modulus. Based on the propagation characteristics of stress wave, the attenuation of incident stress waves in UHMWPE/SSG included three stages, as shown in Fig. 9.

The first stage is the propagation of stress wave in UHMWPE ballistic panel. Because of the ultra-high elastic modulus of UHMWPE, the stress wave showed high propagation velocity and fast attenuation velocity, so the ballistic impact energy could quickly spread outward and be absorbed by UHMWPE. The stress wave propagated along the fiber direction in the UHMWPE sub-laminate, and exhibited different propagation and attenuation velocities due to the anisotropic characteristics of UHMWPE. When the stress wave propagated in the fiber yarn and the free boundary of UHMWPE sub-laminate or to the adjacent UHMWPE sub-laminate, the stress wave energy was greatly dissipated under the combined effect of reflection, transmission and friction of fiber yarn. Hence, the impact energy of 86.46 J was dissipated and absorbed by UHMWPE ballistic panel, and the peak stress was attenuated by 84.13% from 1629.16 MPa to 258.62 MPa.

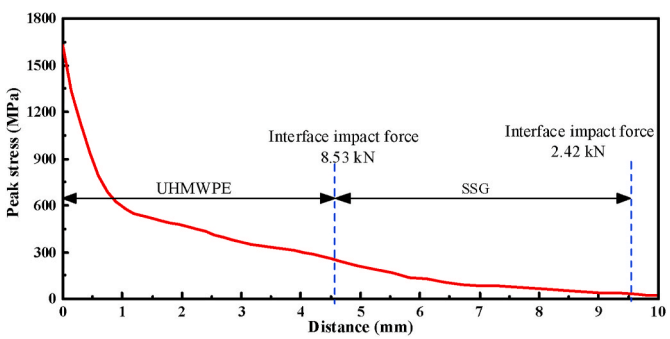

Fig. 9. The attenuation process of stress wave in the UHMWPE/SSG.

The second stage is the propagation of stress wave from UHMWPE to SSG. Although the UHMWPE ballistic laminate absorbed a large amount of ballistic impact energy, part of the ballistic impact energy was still transferred to SSG and EHB in the form of stress waves. Because of the mismatch of elastic impedance, when the stress wave propagated from the high-impedance UHMWPE ballistic laminate to the low-impedance SSG buffer plate, the stress wave velocity and energy were greatly reduced. The stress wave attenuated by 5.67% from 258.62 MPa to 243.95 MPa, and the interface impact force was 8.53 kN.

The final stage is the propagation of stress wave in the SSG. When the stress wave propagated to SSG, the rapid stiffening behavior of SSG made its elastic modulus greatly increase, so that the propagation and attenuation velocity of stress wave showed a significant increase trend. Therefore, more ballistic impact energy was dispersed and absorbed by the stiffened SSG, and the stress wave was attenuated by 85.73% from 243.95 MPa to 34.81 MPa. Eventually, the remaining ballistic impact energy was transferred to EHB, and the interface impact force was also attenuated by 71.63% from 8.53 kN to 2.42 kN.

4.4. Dynamic response process

Fig. 10 shows the dynamic response of ballistic impact model under the protection of UHMWPE/SSG, which could be defined as four distinctive processes.

Firstly, the bullet was upset and deformed by the resistance of CBA during the ballistic impact, its velocity and energy were rapidly attenuated. The impact energy of bullet was continuously transferred to the CBA and EHB, forcing the CBA and EHB to undergo deformation successively, and produce a movement trend along the ballistic impact direction, as shown in Fig. 10a.

Secondly, when the deformation and energy absorption of the UHMWPE sub-laminate exceeded its failure strength, it would be damaged and form a bullet hole slightly larger than the bullet. Then, the bullet continued to impact the subsequent UHMWPE sub-laminate, and the previously damaged UHMWPE sub-laminate began to peel off from the subsequent UHMWPE sub-laminate, eventually resulting in delamination between the UHMWPE sub-laminates, as shown in Fig. 10b.

Thirdly, after the bullet impact was over, UHMWPE ballistic panel continued to impact the SSG by its inertial motion until it separated from the SSG, and then the stretched UHMWPE ballistic panel began to rebound. Similarly, SSG also relied on its inertia motion to further impact the EHB until the maximum bulge deformation of CBA appeared (ie. the impact of CBA on EHB ended), as shown in Fig. 10c. Ultimately, the deformed SSG restored to its original state because of its special property.

Finally, when the impact of CBA on EHB ceased, EHB still had a relatively high residual velocity and continued to compress deformation inward. As a result, a permanent backface signature was formed on the EHB, as shown in Fig. 10d.

4.5. Protective behavior and stiffening mechanism of SSG

The stiffening mechanism of SSG could be clearly explained based on the “Jamming” theory in condensed matter physics [33], as shown in Fig. 11.

During the synthesis of SSG by the polymerization reaction of H_3BO_3 and PDMS-OH, boron (B) atoms are introduced into the molecular chain to obtain three forms of molecular structure, as shown in Fig. 11a. The B atom ($1s^2 2s^2 2p^1$) with missing electrons in the P orbital and the oxygen (O) atom ($1s^2 2s^2 2p^4$) with surplus electrons are attracted to each other, so that a weak B–O crosslink bond (similar to hydrogen bond) is formed between molecular chains. The B–O crosslink bond with weak bond energy is always in a dynamic reversible process of continuous fracture and formation, thus exhibiting impact hardening and self-healing

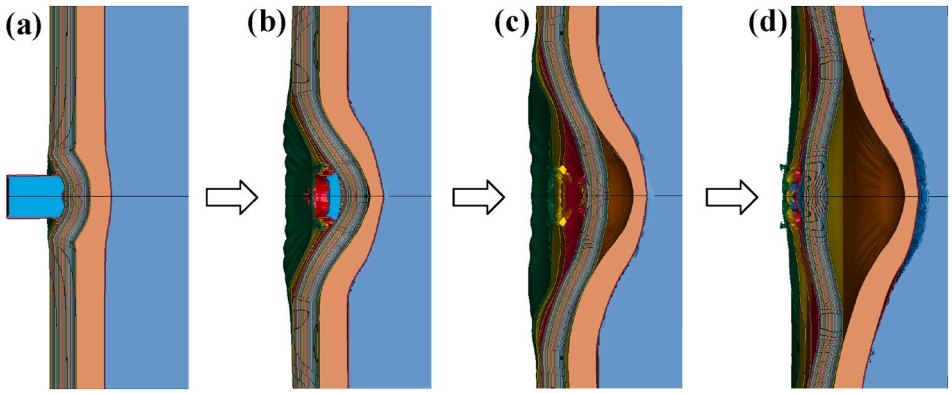

Fig. 10. Dynamic response process: (a) deformation, (b) destruction and stratification, (c) bulge and rebound, (d) formation of backface signature.

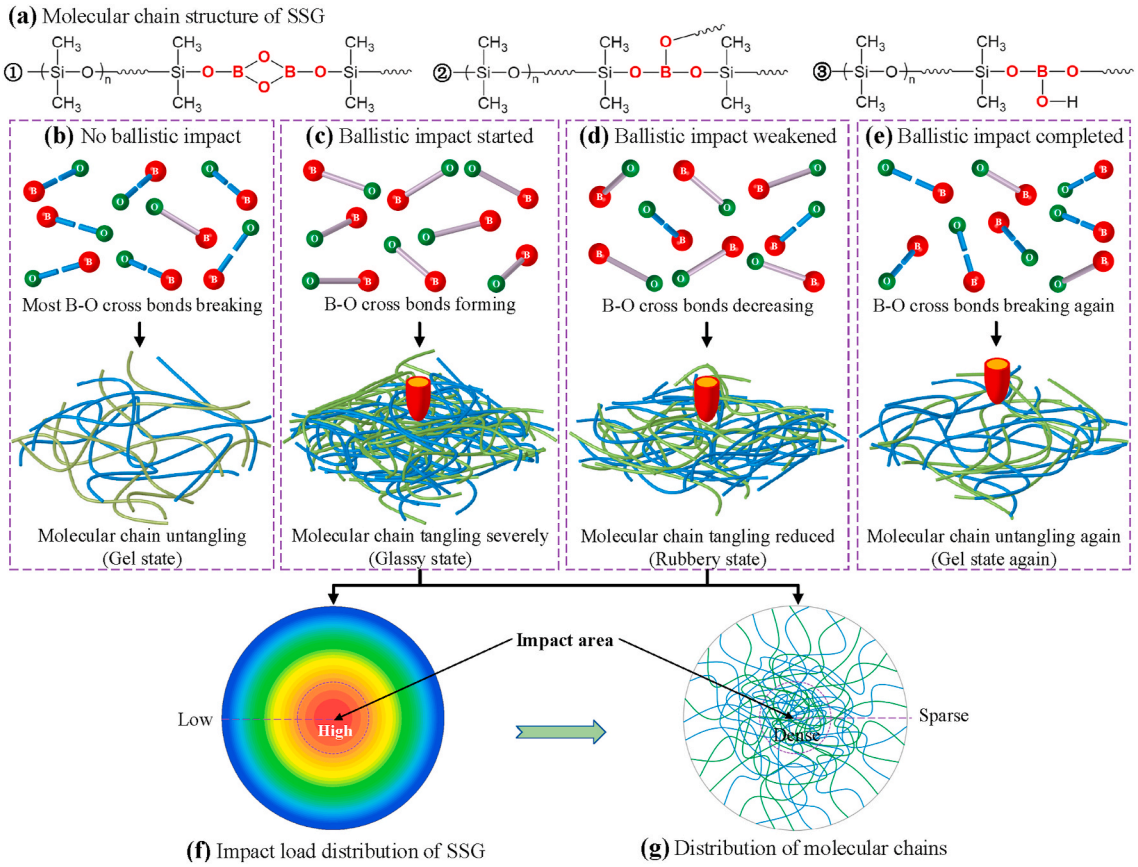

Fig. 11. Stiffening mechanism and process of SSG under ballistic impact.

properties. The formation and fracture of B–O crosslink bonds are affected by impact loads (or strain rate), so the phase change of SSG was defined as four states.

Gel state (Fig. 11b): When CBA was not impacted by bullet, SSG buffer plate was in a static or low shear rate state. The breaking velocity of B–O crosslink bond was greater than the deformation velocity of SSG, resulting in the breaking of most B–O crosslink bonds and the untangling of molecular chains. The weak "Jamming" effect made SSG have low storage modulus and loss modulus, thus showing gel behavior with excellent flexibility.

Glassy state (Fig. 11c): When CBA was impacted by the high-velocity bullet, the effect of the stress wave made the SSG in a high shear rate state to produce relaxation phenomena. Since the breaking velocity of B–O crosslink bond was lower than the deformation velocity of SSG, the B–O crosslink bond did not have enough time to break, so that the molecular chains were severely entangled to enhance the intermolecular force and "Jamming" effect. Therefore, the movement of molecular chain was hindered, causing the SSG to quickly stiffen into the glassy state.

During the ballistic impact, the impact load acting on the SSG presented the distribution law that attenuated from the ballistic impact area to the surroundings, as shown in Fig. 11f. According to the correlation of the impact load of SSG, the entanglement of molecular chains also showed a distribution law from dense to sparse, as shown in Fig. 11g. The severe entanglement of molecular chain increased the internal force (including the force within the molecular chain and the friction between the molecular chains) of molecular chain, which greatly increased the storage modulus and loss modulus of SSG. Finally, the impact resistance

and energy absorption of SSG was significantly enhanced.

Rubbery state (Fig. 11d): As the ballistic impact weakened and the stress wave diffused and decayed in the SSG, the B–O crosslink bond began to break, and the entanglement density and action force of molecular chain also decreased. The weakening of "Jamming" effect forced the SSG to gradually change from the glassy state to the rubbery state.

Gel state again (Fig. 11e): After the ballistic impact, the stress wave gradually dissipated, so SSG was again in a low shear rate. The breaking of most B–O crosslink bonds and the untangling of molecular chains occurred again, causing SSG restored to the gel state.

5. Conclusions

An impact-resistant shear stiffening gel was used as the buffer material for body armor, which was beneficial to further improve the protective performance of body armor. Main conclusions were summarized as follows.

(1) The buffer plate played a vital protective effect in the body armor, and its protective performance was affected by the buffer material. By comparison to the traditional EVA material, SSG dispersed and absorbed more ballistic impact energy, thus greatly reducing the impact force and the bulge deformation of UHMWPE/SSG.
(2) The protective mechanism of SSG was attributed to the rapid phase transition behavior under ballistic impact. The entanglement of SSG molecular chains produced a strong "Jamming" effect, which forced SSG to quickly stiffen to resist deformation and dissipate energy, and ultimately achieved the purpose of protecting the human body.
(3) The stiffening behavior of SSG made the impact force of CBA to change from the "mountain" distribution of high center and low periphery to the "valley" distribution of low center and high periphery, which indicated that the attenuation of ballistic impact energy was positively related to the stiffening degree of SSG.

Author statement

Fan Tang: Investigation, Methodology, Formal analysis, Software, Validation, Writing-original draft. Cheng Dong: Conceptualization, Data curation, Supervision, Validation, Visualization. Zhe Yang: Conceptualization, Methodology, Resources, Supervision. Yue Kang: Methodology, Resources, Visualization, Supervision. Xiancong Huang: Formal analysis, Resources, Investigation. Maohui Li: Conceptualization, Resources, Writing-review & editing. Yuchao Chen: Data curation, Software, Visualization. Wenjian Cao: Methodology, Investigation, Software. Chenguang Huang: Conceptualization, Methodology, Writing-review & editing. Yacong Guo: Project administration, Funding acquisition, Writing-review & editing. Yanpeng Wei: Project administration, Funding acquisition, Writing-review & editing.

Declaration of competing interest

The authors declare that they have no known competing financial interests or personal relationships that could have appeared to influence the work reported in this paper.

Acknowledgments

This work was supported by the National Natural Science Foundation of China (Grant No.12072356 and No.11902329). Fan Tang and Cheng Dong contributed equally in this work.

References

[1] D. Pacek, J. Rutkowski, The composite structure for human body impact protection, Compos. Struct. 265 (2021) 113763.
[2] A. Manero, J. Gibson, G. Freihofer, et al., Evaluating the effect of nano-particle additives in Kevlar® 29 impact resistant composites, Compos. Sci. Technol. 116 (2015) 41–49.
[3] M. Rodríguez-Millán, T. Ito, J.A. Loya, et al., Development of numerical model for ballistic resistance evaluation of combat helmet and experimental validation, Mater. Des. 110 (2016) 391–403.
[4] G. Gopinath, J.Q. Zheng, R.C. Batra, Effect of matrix on ballistic performance of soft body armor, Compos. Struct. 94 (9) (2012) 2690–2696.
[5] L. Gilson, L. Rabet, A. Imad, et al., Experimental and numerical assessment of non-penetrating impacts on a composite protection and ballistic gelatine, Int. J. Impact Eng. 136 (2020) 103417.
[6] Y. Wen, C. Xu, S. Wang, et al., Analysis of behind the armor ballistic trauma, J. Mech. Behav. Biomed. Mater. 45 (2015) 11–21.
[7] L. Chang, Y. Guo, X. Huang, et al., Experimental study on the protective performance of bulletproof plate and padding materials under ballistic impact, Mater. Des. 207 (2021) 109841.
[8] S. Cao, H. Pang, C. Zhao, et al., The CNT/PSt-EA/Kevlar composite with excellent ballistic performance, Compos. B Eng. 185 (2020) 107793.
[9] J. Qin, B. Guo, L. Zhang, et al., Soft armor materials constructed with Kevlar fabric and a novel shear thickening fluid, Compos. B Eng. 183 (2020) 107686.
[10] S. Gürgen, A. Sert, Polishing operation of a steel bar in a shear thickening fluid medium, Compos. B Eng. 175 (2019) 107127.
[11] S.R. Waitukaitis, H.M. Jaeger, Impact-activated solidification of dense suspensions via dynamic jamming fronts, Nature 487 (7406) (2012) 205–209.
[12] Z. Lu, X. Jing, B. Sun, et al., Compressive behaviors of warp-knitted spacer fabrics impregnated with shear thickening fluid, Compos. Sci. Technol. 88 (2013) 184–189.
[13] Y. Kim, S.K. Sathish Kumar, Y. Park, et al., High-velocity impact onto a high-frictional fabric treated with adhesive spray coating and shear thickening fluid impregnation, Compos. B Eng. 185 (2020) 107742.
[14] R. Bai, Y. Ma, Z. Lei, et al., Energy analysis of fabric impregnated by shear thickening fluid in yarn pullout test, Compos. B Eng. 174 (2019) 106901.
[15] Q. Zhang, Z. Qin, R. Yan, et al., Processing technology and ballistic-resistant mechanism of shear thickening fluid/high-performance fiber-reinforced composites: a review, Compos. Struct. 266 (2021) 113806.
[16] K. Fu, H. Wang, L. Chang, et al., Low-velocity impact behaviour of a shear thickening fluid (STF) and STF-filled sandwich composite panels, Compos. Sci. Technol. 165 (2018) 74–83.
[17] X. Liu, C. Qian, K. Yu, et al., Energy absorption and low-velocity impact response of shear thickening gel reinforced polyurethane foam, Smart Mater. Struct. 29 (2020), 045018.
[18] S. Zhang, S. Wang, T. Hu, et al., Study the safeguarding performance of shear thickening gel by the mechanoluminescence method, Compos. B Eng. 180 (2020) 107564.
[19] C. Zhao, X. Gong, S. Wang, et al., Shear stiffening gels for intelligent anti-impact applications, Cell Rep. Phys. Sci. 1 (12) (2020) 1–19.
[20] C. Zhao, Y. Wang, S. Cao, et al., Conductive shear thickening gel/Kevlar wearable fabrics: a flexible body armor with mechano-electric coupling ballistic performance, Compos. Sci. Technol. 182 (2019) 107782.
[21] C. Xu, Y. Wang, J. Wu, et al., Anti-impact response of Kevlar sandwich structure with silly putty core, Compos. Sci. Technol. 153 (2017) 168–177.
[22] Y. Wang, S. Wang, C. Xu, et al., Dynamic behavior of magnetically responsive shear-stiffening gel under high strain rate, Compos. Sci. Technol. 127 (2016) 169–176.
[23] Y. Wang, X. Gong, S. Xuan, Study of low-velocity impact response of sandwich panels with shear-thickening gel cores, Smart Mater. Struct. 27 (2018), 065008.
[24] X. Liu, K. Yu, Q. Fu, et al., Shear thickening gel reinforced flexible polyurethane foam and its enhanced properties, Smart Mater. Struct. 28 (2019), 055017.
[25] Q. He, S. Cao, Y. Wang, et al., Impact resistance of shear thickening fluid/Kevlar composite treated with shear-stiffening gel, Compos. Appl. Sci. Manuf. 106 (2018) 82–90.
[26] F. Tang, Z. Guo, M. Yuan, et al., Mechanical response of human torso under blast loading, Saf. Sci. 131 (2020) 104936.
[27] D.B. Rahbek, J.W. Simons, B.B. Johnsen, et al., Effect of composite covering on ballistic fracture damage development in ceramic plates, Int. J. Impact Eng. 99 (2017) 58–68.
[28] S. Gao, B. Chen, Effect of UHMWPE fiber laminate on effective protection area of ceramic composite target, Key Eng. Mater. Trans. Tech. Publ. (2019) 133–138.
[29] X. Liu, M. Li, X. Li, et al., Ballistic performance of UHMWPE fabrics/EAMS hybrid panel, J. Mater. Sci. 53 (10) (2018) 7357–7371.
[30] F. Penta, G. Amodeo, A. Gloria, et al., Low-velocity impacts on a polymeric foam for the passive safety improvement of sports fields: meshless approach and experimental validation, Appl. Sci. 8 (7) (2018) 1174.
[31] C. Hernandez, A. Maranon, I.A. Ashcroft, et al., A computational determination of the Cowper–Symonds parameters from a single Taylor test, Appl. Math. Model. 37 (7) (2013) 4698–4708.
[32] D. Luo, Y. Wang, F. Wang, et al., The influence of metal cover plates on ballistic performance of silicon carbide subjected to large-scale tungsten projectile, Mater. Des. 191 (2020) 108659.
[33] E. Han, I.R. Peters, H.M. Jaeger, High-speed ultrasound imaging in dense suspensions reveals impact-activated solidification due to dynamic shear jamming, Nat. Commun. 7 (1) (2016) 1–8.